

Tensor-network approach to quantum optical state evolution beyond the Fock basis

Nikolay Kapridov,^{1,2,*} Egor Tiunov,^{3,†} and Dmitry Chermoshentsev^{1,2,‡}

¹*Moscow Institute of Physics and Technology,
Dolgoprudny, Moscow Region 141700, Russia*

²*Russian Quantum Center, Skolkovo, Moscow 121205, Russia*

³*Quantum Research Center, Technology Innovation Institute, Abu Dhabi, UAE*

Understanding the quantum evolution of light in nonlinear media is central to the development of next-generation quantum technologies. Yet, modeling these processes remains computationally demanding, as the required resources grow rapidly with photon number and phase-space resolution. Here, we introduce a tensor-network approach that efficiently captures the dynamics of nonlinear optical systems in a continuous-variable representation. Using the matrix product state (MPS) formalism, both quantum states and operators are encoded in a highly compressed form, enabling direct numerical integration of the Schrödinger equation. We demonstrate the method by simulating degenerate spontaneous parametric down-conversion (SPDC) and show that it accurately reproduces established theoretical benchmarks—energy conservation, pump depletion, and quadrature squeezing—even in regimes where conventional Fock-basis simulations become infeasible. For high-intensity pump fields ($\alpha = 100$), the MPS representation achieves compression ratios above $3 \cdot 10^3$ while preserving physical fidelity. This framework opens a scalable route to modeling multi-mode quantum light and nonlinear optical phenomena beyond the reach of traditional methods.

I. INTRODUCTION

Optical and photonic devices with nonlinear properties are rapidly advancing, finding widespread applications in quantum technologies [1, 2]. To ensure their effective implementation, it is essential to predict the behavior of optical quantum states under different conditions. However, the simulation of the quantum state dynamics is a challenging task because of the high dimensionality of the Hilbert space [3]. This challenge motivates the development of new simulation techniques to limit the rapid growth of required computational resources with the Hilbert-space dimension. Simulating a quantum state’s evolution involves solving the Schrödinger equation, which requires selecting a representation of the state. A commonly accepted strategy is to represent optical quantum states in discrete Fock basis. This basis is infinite, however, it is typically truncated to a finite subspace in practice [4, 5]. Alternatively, wavefunctions can be represented in a continuous basis [6, 7]. In the numerical simulation, continuous variables are discretized to the extent necessary to resolve all the details of the encoded wavefunction.

It turns out that describing continuous wave functions with exponentially high resolution is possible with the help of tensor networks. One of the most effective and widely used types of tensor networks is the Matrix Product State (MPS) [8–14].

It has proven to be an efficient ansatz for ground states of gapped 1D Hamiltonians [15–17]. The MPS representation was independently discovered by the math community under the name of Tensor Train (TT) [18]. Various linear algebraic methods were reimplemented within the TT framework [18–20]. Several studies have investigated the key properties of grid-discretized functions that allow their efficient representation within tensor-network formats. In particular, it has been shown that exponential, trigonometric, and polynomial functions can be analytically expressed in the TT form [21]. Moreover, a direct connection has been established between the internal complexity of a tensor-network representation and the smoothness of the encoded function [22]. Thus, the tensor network approach opens an attractive avenue to simulate high-dimensional continuous problems efficiently and at scale [23–29].

In this work, we focus on simulating the quantum evolution of optical processes by solving the Schrödinger equation. When the system is initialized with a large number of photons—for example, when a nonlinear medium is driven by a laser field of high intensity—the corresponding cutoff in the Fock space must be increased to accurately capture all relevant photon-number components. This, in turn, leads to a rapid growth of the Hilbert-space dimension, making direct simulations computationally intensive due to memory and processing-time limitations.

Here, we address this challenge for the degenerate spontaneous parametric down-conversion (SPDC) process by combining the continuous-variable formulation of its quantum evolution with the MPS

* kapridov.na@phystech.edu

† egor.tiunov@tii.ae

‡ dac@rqc.ru

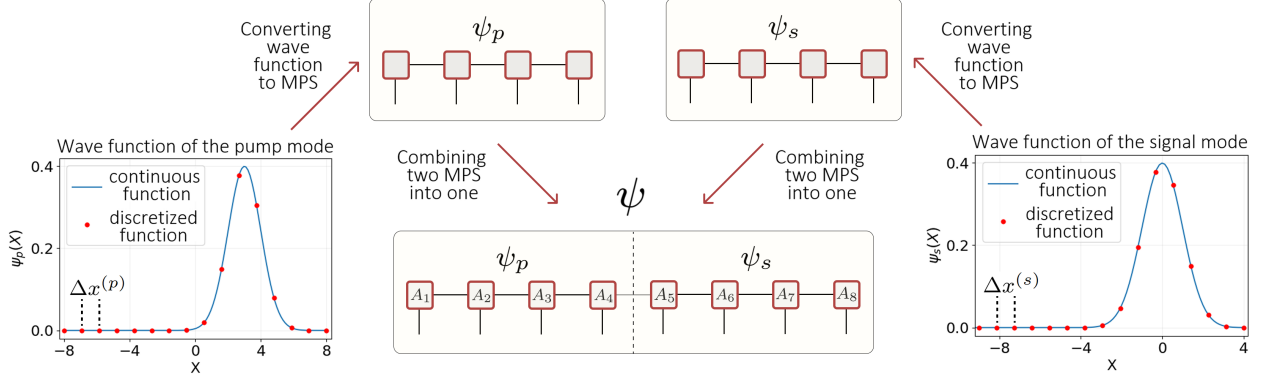


FIG. 1. Encoding the wave function of the entire system in the MPS representation. Wave function of each mode is discretized with the required precision. Then it is converted to the MPS format. After that, the MPS of the entire system is assembled from stacking MPS tensors of each mode. In this example, the wave function of the pump mode is determined on the segment $R^{(p)} = [-8, 8]$, signal mode - on the segment $R^{(s)} = [-9, 4]$. Each mode is discretized with $N = 16$ points which corresponds to a MPS with 4 tensors (for each mode). The MPS of entire system contains 8 tensors.

representation. Accurate resolution of the wavefunction's fine structure—rapid phase oscillations, interference fringes, and non-Gaussian tails—requires a large phase-space window and a finely sampled grid, yielding a high-dimensional discretization. To keep the computations tractable, we employ the MPS representation, which compactly factorizes the state while preserving the essential correlations. We validate the accuracy of our approach by simulating the SPDC process with the pump mode initialized in a coherent state $\alpha = 10$ in the Fock basis using sparse-matrix methods. We then extend the analysis to a higher amplitude $\alpha = 100$, which more closely reflects experimental conditions where a laser mode typically contains thousands to millions of photons within its coherence volume. To validate the proposed algorithm, we introduce a set of benchmark metrics—total energy conservation, pump depletion, variance of the X -quadrature, and numerical error analysis. Since direct benchmarking with the full Fock basis is computationally infeasible, these metrics serve as reliable indicators of simulation accuracy. According to these criteria, the MPS-based simulations faithfully reproduce the expected quantum dynamics, confirming the validity of the proposed approach.

II. METHODS

In this paper, we tackle the problem of quantum state evolution governed by the Hamiltonian of the SPDC process in the continuous quadrature basis. In the interaction picture, the Hamiltonian is expressed in terms of photon creation (\hat{a}^\dagger) and annihilation (\hat{a}) operators as follows:

lution (\hat{a}) operators as follows:

$$\hat{H} = i\kappa(\hat{a}_p^\dagger \hat{a}_s \hat{a}_s - \hat{a}_p \hat{a}_s^\dagger \hat{a}_s^\dagger) \quad (1)$$

Here, κ is the coupling constant, which is proportional to the second-order nonlinear susceptibility $\chi^{(2)}$. The subscripts p and s denote the pump and signal modes, respectively. In the quadrature representation, the creation and annihilation operators are given by:

$$\begin{cases} \hat{a}^\dagger = \frac{X - d/dX}{\sqrt{2}} \\ \hat{a} = \frac{X + d/dX}{\sqrt{2}} \end{cases} \quad (2)$$

To simulate the quantum evolution of the system, we numerically solve the time-dependent Schrödinger equation using the implicit Euler method:

$$(\hat{I} - i\Delta t \hat{H})\psi_{t+1}(x) - \psi_t(x) = 0, \quad (3)$$

where \hat{I} stands for the identity matrix, Δt is the time step, $\psi_t(x)$ is the wavefunction in the position x at time t .

The Schrödinger equation (3) defines a linear system for the wavefunction at time step $t + 1$. The signal (s) and pump (p) components of the wavefunction are discretized on predefined grids of size $N^{(s/p)}$ and resolution $\Delta x^{(s/p)}$ (see Fig. 1). The grid spacing is chosen to resolve all fine-scale features of the continuous wavefunction throughout the entire evolution. The spatial support of each component, $[x_a^{(s/p)}, x_b^{(s/p)}]$, is selected such that the wavefunction remains negligible outside this interval at all times.

To facilitate the encoding of wavefunctions and operators in MPS format, the grid size is required to be a power of two, i.e., $N = 2^n$.

We consider the pump and the signal modes as a closed quantum system. Consequently, the corresponding wavefunction captures all information and correlations between the two modes in a single vector of size $N^{(p)} \times N^{(s)}$. The initial state of the system, denoted by ψ_0 , is taken as a tensor product of a vacuum state for the signal mode, $\psi_0^{(s)}(x)$, and a coherent state for the pump mode, $\psi_0^{(p)}(x)$, respectively:

$$\psi_0^{(s)}(x) = \pi^{-1/4} \exp\{-x^2/2\} \quad (4)$$

$$\psi_0^{(p)}(x) = \pi^{-1/4} \exp\{-(x-x_0)^2/2\} \quad (5)$$

$x_0 = \alpha\sqrt{2}$, where α is the amplitude of the coherent state.

The novelty of our approach is encoding both the Hamiltonian and the overall wave function of the system in the MPS representation [18, 30] and solving the Schrödinger equation written in the quadrature basis directly within this framework. To enable this, we begin by expressing the discretized support of the wavefunction in binary representation. Specifically, each grid point x_k is uniquely indexed by a binary string (i_1, i_2, \dots, i_n) , where $i_j \in 0, 1$. This allows us to rewrite the wavefunction as:

$$|\psi\rangle = \sum_k \psi(x_k) |x_k\rangle \Delta x = \sum_{i_1 \dots i_n} \psi_{i_1 \dots i_n} |i_1 \dots i_n\rangle \quad (6)$$

Afterwards, we utilize the MPS as an ansatz to approximate the tensor of complex amplitudes $\psi_{i_1 \dots i_n}$ in a compressed way:

$$\psi_{i_1 \dots i_n} = \sum_{\alpha_0, \dots, \alpha_n} A_{\alpha_0 i_1 \alpha_1}^{[1]} A_{\alpha_1 i_2 \alpha_2}^{[2]} \dots A_{\alpha_{n-1} i_n \alpha_n}^{[n]}. \quad (7)$$

Here $A_{\alpha_{j-1} i_j \alpha_j}^{[j]}$ are elements of a three-dimensional tensor $A^{[j]}$ of shape $(r_{j-1}, 2, r_j)$, $r_0 = r_n = 1$. Index i_j of tensor $A^{[j]}$ matches the corresponding bit in the binary notation (6) and is responsible for selecting one of the two matrices $\{A_0^{[j]}, A_1^{[j]}\}$ of shape (r_{j-1}, r_j) . In notation (6), each bit value i_j dictates the behavior of the wave function across distinct scales: the index i_1 selects between the first or the second half of the wave function support, while the index i_2 splits the first selected half into two halves again, and so on down to finer resolutions. In the MPS representation, this multiscale structure is encoded in the corresponding tensors. Fixing the value of index i_j for each tensor $A^{[j]}$ and multiplying the corresponding matrices allows to compute

one element of the original wave function. The sizes r_j of the matrices $A_{r_{j-1} i_j r_j}^{[j]}$, called bond dimensions, determine how distinct scales are correlated between each other.

To encode the initial wavefunction of the full system into a tensor network, we first convert the discretized initial wavefunctions of the pump (5) and signal (4) into MPS. These two MPS representations are then sequentially stacked to form the composite state of the entire system at time $t = 0$ (see Fig. 1). The system Hamiltonian (1) is expressed as a sum of tensor products of creation and annihilation operators, \hat{a} and \hat{a}^\dagger . Since each of these operators can be efficiently represented as a matrix product operator (MPO) (see Appendix), the full Hamiltonian is constructed by combining the MPOs corresponding to different modes via appropriate tensor products. Furthermore, elementwise products and linear combinations of MPOs can also be carried out efficiently within the MPS formalism [30]. Once both the operator $\hat{U} \equiv (\hat{I} - i\Delta t \hat{H})$ and the wavefunction $\psi(x)$ are expressed in MPS form, the linear system

$$\hat{U}\psi_{t+1} = \psi_t \quad (8)$$

arising from the time-stepping scheme (3) can be solved using a DMRG-style variational algorithm [20] (see Appendix for the details).

The MPS representation of continuous and smooth functions is not conventional for the quantum-optical community. However, there are several well-established reasons why such a representation admits low bond dimension structure. First, smoothness suppresses high-frequency components, implying that the function can be well-approximated using a small number of Fourier harmonics [22, 32]. Each harmonic term can be written as an exponential function, implying that it has a bond dimension equal to 1. Second, many analytic or highly differentiable functions are sparse in orthogonal polynomial bases, such as Chebyshev polynomials. In such cases, the MPS representation of each basis function is a low-rank tensor: for example, a Chebyshev polynomial of degree N has bond dimension bounded by $N+1$ [22, 33]. Smoothness implies that a function can be well-approximated by low-degree polynomials. In the MPS representation, where input variables correspond to binary digits of the domain, this means that the function's variation within each interval is locally simple and requires only low-rank structure to represent. As shown by Lindsey [22], this leads to decaying MPS ranks with depth—since deeper binary digits (finer intervals) capture increasingly less complex behavior, the corresponding MPS tensors become smaller. Consequently, the interaction between different digit groups remains low-dimensional, and the overall MPS representation

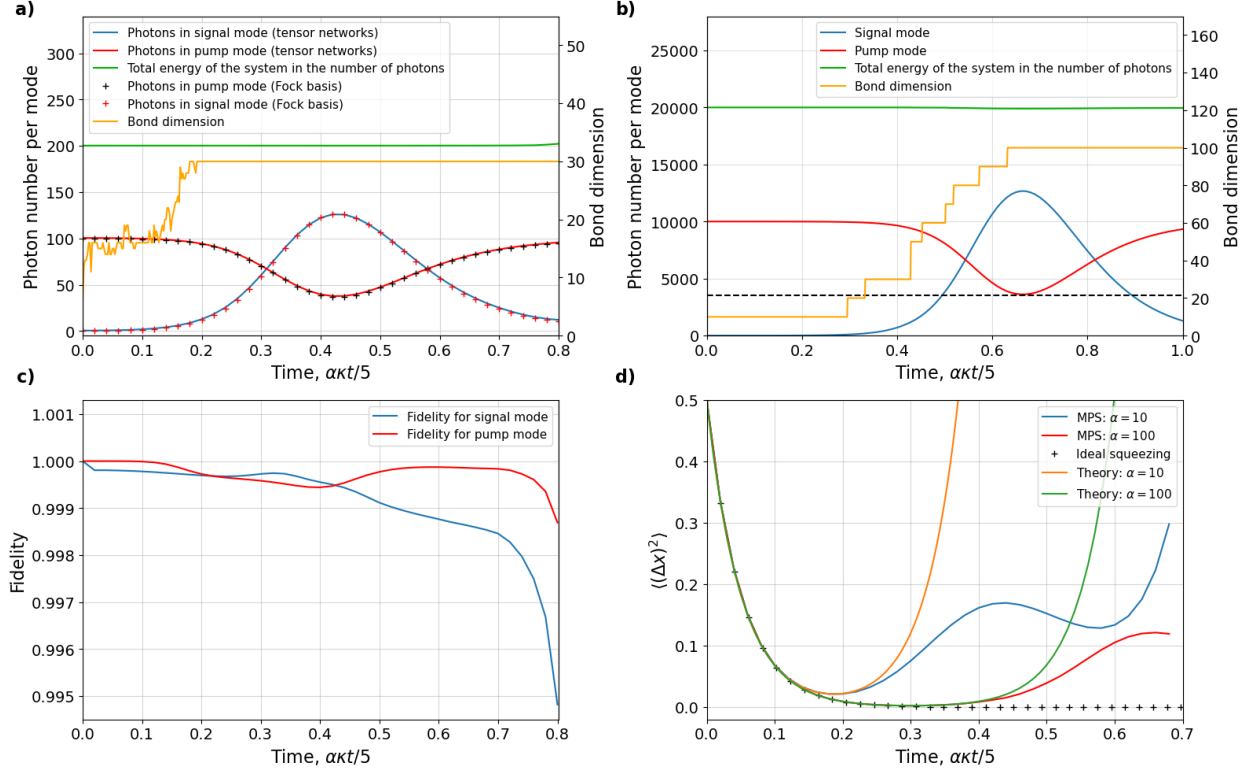


FIG. 2. **(a,b)** Photon population dynamics $\langle n \rangle = \text{Tr}(\rho a^\dagger a)$ in the pump and signal modes (left Y-axis) and bond dimension change (right Y-axis) during quantum evolution in the SPDC process. Blue and red solid lines correspond to the MPS algorithm; green line shows total energy of the system expressed in the number of signal photons; orange solid line demonstrates how the bond dimension changes during the evolution. **(a)** Pump mode is initialized in the coherent state $\alpha = 10$. Crossed dots demonstrate state vector simulation in Fock basis. **(b)** Pump mode is initialized in the coherent state $\alpha = 100$. Black dashed line shows the theoretical limit of pump mode depletion. **(c)** Fidelity between Fock-basis state-vector and continuous-basis MPS simulations of the signal and pump density matrices during the quantum evolution. Fidelity calculation is done in the Fock basis. **(d)** Variance of X -quadrature in the signal mode during quantum evolution with the pump mode initialized at $\alpha = 10$ and $\alpha = 100$. The blue and red lines demonstrate MPS approach, while orange and green lines correspond to the theoretical analysis given in Ref. [31]. The black crosses indicate variance for the ideal single-mode squeezing in the parametric approximation (pump mode is treated as a classical field).

stays compact.

III. RESULTS

To validate our framework, we compare two approaches: (i) Fock-basis simulations using the standard state-vector representation and (ii) continuous-variable simulations employing an MPS ansatz. The pump mode is initialized in a coherent state with amplitude $\alpha = 10$, which requires a Fock-basis cutoff of about 150 photons, which is still tractable for state-vector methods. For the tensor-network simulation, the signal and the pump modes are initialized with the parameters from the first ($\alpha = 10$) column of the Table I.

Fig. 2 **(a)** demonstrates photon dynamics in pump

	$\alpha = 10$	$\alpha = 100$
R_s	[-10,10]	[-10,10]
R_p	[-24,24]	[-151,151]
n_p	12	15
n_s	13	15
$n_{mps} = n_p + n_s$	25	30
$x_0 = \sqrt{2}\alpha$	14.1	141

TABLE I. Parameters used for tensor network simulations: R_s (R_p) is a spatial support for the signal (pump) mode, n_s (n_p) stands for the number of bits in the signal (pump) mode, n_{mps} denotes the number of bits in the overall wavefunction, x_0 is the mean coordinate of the coherent state at the initial time moment.

($\langle n_p \rangle = \text{Tr}(\rho_p a_p^\dagger a_p)$) and signal ($\langle n_s \rangle = \text{Tr}(\rho_s a_s^\dagger a_s)$) modes during evolution, obtained from the numeri-

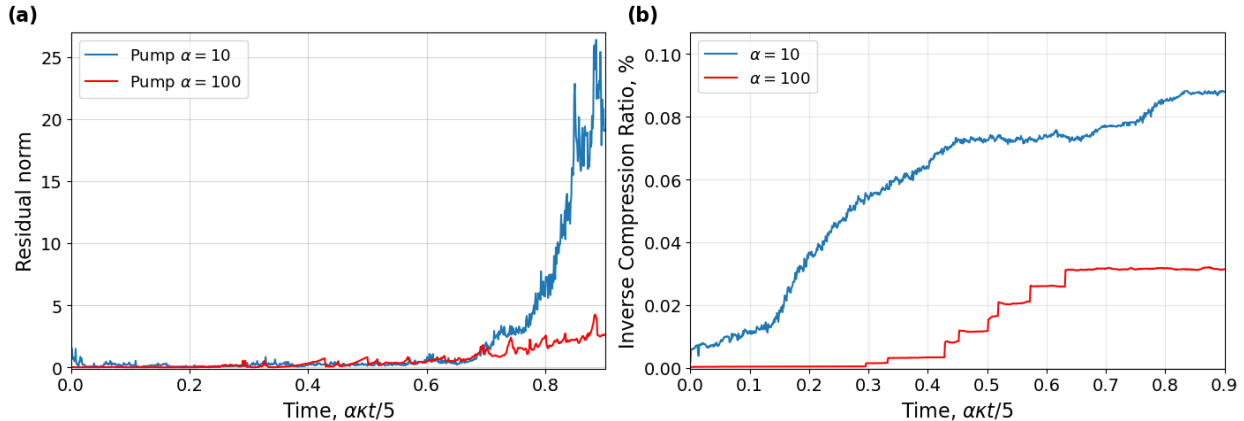


FIG. 3. **(a)** l_2 residual norm $\|\tilde{\psi}_t - U\tilde{\psi}_{t+1}\|/\sqrt{\mathcal{N}}$ of the linear system (3) during the quantum evolution simulation, for pump mode initialized at $\alpha = 10$ ($\mathcal{N} = 1$) and $\alpha = 100$ ($\mathcal{N} = 2^5$). **(b)** Inverse compression ratio. The ratio between the total number of elements in MPS and the mesh size throughout the SPDC evolution. Blue (red) line corresponds to the case when the pump mode is initialized in a coherent state $\alpha = 10$ ($\alpha = 100$).

cal simulations in both the Fock basis and the continuous representation using MPS (see red and blue curves, respectively). The two approaches yield identical results throughout the entire evolution. The correctness of the MPS-based simulations is also confirmed by the conservation of the total number of photons (energy), which corresponds to the green line in Fig. 2 (a). Fig. 2 (a) also demonstrates the maximum bond dimension of MPS throughout the quantum evolution (yellow line). It grows up to 30, which is set as the truncation cutoff. This value is enough since the fidelity between the density matrices obtained using CV-MPS method and the exact Fock-basis method is more than 0.994% for both signal and pump modes (see Fig. 2 (c)).

Then we switch to the regime where the pump mode is initialized in a coherent state with amplitude $\alpha = 100$. Computation in the Fock basis is infeasible on our hardware (Intel Core i7-10700 CPU @ 2.90 GHz, 32 GB RAM) even when using sparse linear algebra operations, since it requires solving a linear system in a vector space of dimension around 10^8 for each timestep. For this scenario, we adjusted all parameters of the signal and the pump modes according to the second ($\alpha = 100$) column of the Table I.

Fig. 2(b) (red and blue lines) shows photon-number dynamics in the pump and signal modes during quantum evolution. In this case, we have no direct reference to compare our results with, for the reasons discussed in the previous paragraph. Therefore, to validate our algorithm, we present four figures of merit: total energy conservation, benchmarks for pump depletion, variance of X -quadrature, and numerical error analysis. We begin with the en-

ergy conservation: since we are modeling a closed quantum system, we make sure that the total energy of the system is conserved as demonstrated in the Fig. 2(b) by the green line. Next, theoretical studies of the SPDC process report an energy transfer limit from the pump to the signal mode of about 65–66%[34, 35]. The black horizontal dotted line in the Fig. 2(b) represents this limit and closely matches the maximum depletion of the pump mode observed in our simulation. In addition, the variance of the squeezed quadrature for different initial pump-mode amplitudes has been theoretically derived using perturbation theory in previous studies[31, 36, 37]. The corresponding theoretical curves for pump amplitudes $\alpha = 10$ and $\alpha = 100$ are shown in the Fig. 2(d) in orange and green, respectively. These curves are determined by the two leading terms of the perturbation series and are valid while $\exp\{(2\alpha\kappa t)\} \ll 16\alpha^2/3$ (see Ref. [31]), which include the point of maximum quadrature squeezing. They coincide with our computations at least up to this point. Finally, in Fig. 3(a), we compute the l_2 residual norm of the linear system $\|\tilde{\psi}_t - U\tilde{\psi}_{t+1}\|/\sqrt{\mathcal{N}}$, as a function of time. The residual is normalized by the factor $\mathcal{N} = 2^{30-25}$ for $\alpha = 100$ so that it doesn't depend on the discretization of the x -axis. The error observed for $\alpha = 100$ is quantitatively similar to that for $\alpha = 10$. Since our calculations match with the simulation in Fock basis for $\alpha = 10$, this fact supports the reliability of the results obtained for the higher value of α .

The computation with the pump mode initialized at $\alpha = 100$ becomes feasible due to the compression capability of the MPS ansatz. To quantify it, we compute the inverse compression ratio at each step

of the quantum evolution (see Fig. 3(b)). This ratio, defined as the total number of elements in the MPS tensors divided by the mesh size (2^n), displays the compression efficiency of MPS compared to the standard vector representation. Throughout the entire evolution, this ratio exceeds $3 \cdot 10^3$ for $\alpha = 100$ and more than 10^3 for $\alpha = 10$.

IV. CONCLUSION AND OUTLOOK

We present a novel numerical approach for modeling the evolution of quantum optical states. Our method uses a discretized continuous representation of states and operators, which are then encoded in the MPS format. The entire algorithm operates within the MPS framework, eliminating the need for going back to the dense vector representation. To validate our approach, we compared quantum evolution simulations of the SPDC process in the Fock basis and in the continuous representation using tensor networks. Both approaches match each other in a low-amplitude regime ($\alpha = 10$). Remarkably, our technique enables simulations of quantum states containing thousands of photons per mode, a regime where traditional methods face significant challenges. In the absence of direct benchmarks for

$\alpha = 100$, the MPS ansatz demonstrated good agreement with the several sanity checks: energy conservation, consistency with the previous theoretical investigations, the level of pump depletion, and the value of the numerical discrepancy arising from the solution of linear systems.

This work lays the groundwork for subsequent studies aimed at simulating quantum effects in optical ring microresonators[38, 39]. In particular, future efforts will focus on modeling multimode quantum optical evolution in media with $\chi^{(2)}$ and $\chi^{(3)}$ nonlinearities[40–43]. While the current framework provides an effective method for simulating quantum evolution, further refinement of the time-stepping scheme is needed to scale up the technique to multiple modes. One of the promising directions here is time dependent variational principle formulated in MPS format[44–46]. Additionally, other types of tensor networks can potentially be implemented, for example, Tucker representation[47, 48] or tree tensor networks in general[49]. Overall, the proposed framework provides a scalable and conceptually transparent route toward simulating and optimizing high-dimensional quantum systems, bridging the gap between classical tensor-network algorithms and current quantum optical technologies.

-
- [1] Taira Giordani, Francesco Hoch, Gonzalo Carvacho, Nicolò Spagnolo, and Fabio Sciarrino. Integrated photonics in quantum technologies. *La Rivista del Nuovo Cimento*, 46(2):71–103, 2023.
 - [2] Jianwei Wang, Fabio Sciarrino, Anthony Laing, and Mark G Thompson. Integrated photonic quantum technologies. *Nature Photonics*, 14(5):273–284, 2020.
 - [3] Richard P Feynman. Simulating physics with computers. In *Feynman and computation*, pages 133–153. cRc Press, 2018.
 - [4] Karthik Chinni and Nicolás Quesada. Beyond the parametric approximation: Pump depletion, entanglement, and squeezing in macroscopic down-conversion. *Physical Review A*, 110(1):013712, 2024.
 - [5] SP Nikitin and AV Masalov. Quantum state evolution of the fundamental mode in the process of second-harmonic generation. *Quantum Optics: Journal of the European Optical Society Part B*, 3(2):105, 1991.
 - [6] Alexander I Lvovsky and Michael G Raymer. Continuous-variable optical quantum-state tomography. *Reviews of modern physics*, 81(1):299–332, 2009.
 - [7] Ekaterina Fedotova, Nikolai Kuznetsov, Egor Tiunov, AE Ulanov, and AI Lvovsky. Continuous-variable quantum tomography of high-amplitude states. *Physical Review A*, 108(4):042430, 2023.
 - [8] Steven R White. Density matrix formulation for quantum renormalization groups. *Physical review letters*, 69(19):2863, 1992.
 - [9] Steven R White. Density-matrix algorithms for quantum renormalization groups. *Physical review b*, 48(14):10345, 1993.
 - [10] Stellan Östlund and Stefan Rommer. Thermodynamic limit of density matrix renormalization. *Physical review letters*, 75(19):3537, 1995.
 - [11] Stefan Rommer and Stellan Östlund. Class of ansatz wave functions for one-dimensional spin systems and their relation to the density matrix renormalization group. *Physical review b*, 55(4):2164, 1997.
 - [12] David Perez-Garcia, Frank Verstraete, Michael M Wolf, and J Ignacio Cirac. Matrix product state representations. *arXiv preprint quant-ph/0608197*, 2006.
 - [13] Jorge Dukelsky, Miguel A Martín-Delgado, Tomotshi Nishino, and Germán Sierra. Equivalence of the variational matrix product method and the density matrix renormalization group applied to spin chains. *Europhysics letters*, 43(4):457, 1998.
 - [14] Frank Verstraete and J Ignacio Cirac. Matrix product states represent ground states faithfully. *Physical Review B—Condensed Matter and Materials Physics*, 73(9):094423, 2006.
 - [15] Daniel Jaschke, Simone Montangero, and Lincoln D Carr. One-dimensional many-body entangled open

- quantum systems with tensor network methods. *Quantum science and technology*, 4(1):013001, 2018.
- [16] Matthew B Hastings. Solving gapped hamiltonians locally. *Physical Review B—Condensed Matter and Materials Physics*, 73(8):085115, 2006.
- [17] Bogdan Pirvu, Guifre Vidal, Frank Verstraete, and Luca Tagliacozzo. Matrix product states for critical spin chains: Finite-size versus finite-entanglement scaling. *Physical Review B—Condensed Matter and Materials Physics*, 86(7):075117, 2012.
- [18] Ivan V Oseledets. Tensor-train decomposition. *SIAM Journal on Scientific Computing*, 33(5):2295–2317, 2011.
- [19] Ivan Oseledets. Compact matrix form of the d-dimensional tensor decomposition. *IEICE Proceedings Series*, 43(B2L-C2), 2009.
- [20] Ivan V Oseledets and Sergey V Dolgov. Solution of linear systems and matrix inversion in the ttf-format. *SIAM Journal on Scientific Computing*, 34(5):A2718–A2739, 2012.
- [21] Boris N Khoromskij. O ($d \log n$)-quantics approximation of n-d tensors in high-dimensional numerical modeling. *Constructive Approximation*, 34:257–280, 2011.
- [22] Michael Lindsey. Multiscale interpolative construction of quantized tensor trains. *arXiv preprint arXiv:2311.12554*, 2023.
- [23] Nikita Gourianov, Michael Lubasch, Sergey Dolgov, Quincy Y van den Berg, Hessam Babae, Peyman Givi, Martin Kiffner, and Dieter Jaksch. A quantum-inspired approach to exploit turbulence structures. *Nature Computational Science*, 2(1):30–37, 2022.
- [24] Raghavendra Dheeraj Peddinti, Stefano Pisoni, Alessandro Marini, Philippe Lott, Henrique Argentero, Egor Tiunov, and Leandro Aolita. Quantum-inspired framework for computational fluid dynamics. *Communications Physics*, 7(1):135, 2024.
- [25] Stefano Pisoni, Raghavendra Dheeraj Peddinti, Egor Tiunov, Siddhartha E Guzman, and Leandro Aolita. Compression, simulation, and synthesis of turbulent flows with tensor trains. *arXiv preprint arXiv:2506.05477*, 2025.
- [26] Raghavendra Dheeraj Peddinti, Stefano Pisoni, Narsimha Rapaka, Mohamed K Riahi, Egor Tiunov, and Leandro Aolita. Quantum-inspired space-time pde solver and dynamic mode decomposition. *arXiv preprint arXiv:2510.21767*, 2025.
- [27] Martin Kiffner and Dieter Jaksch. Tensor network reduced order models for wall-bounded flows. *Physical Review Fluids*, 8(12):124101, 2023.
- [28] Egor Kornev, Sergey Dolgov, Karan Pinto, Markus Pflitsch, Michael Perelshtein, and Artem Melnikov. Numerical solution of the incompressible navier-stokes equations for chemical mixers via quantum-inspired tensor train finite element method. *arXiv preprint arXiv:2305.10784*, 2023.
- [29] Lucas Arenstein, Martin Mikkelsen, and Michael Kastoryano. Fast and flexible quantum-inspired differential equation solvers with data integration. *arXiv preprint arXiv:2505.17046*, 2025.
- [30] Ulrich Schollwöck. The density-matrix renormalization group in the age of matrix product states. *Annals of physics*, 326(1):96–192, 2011.
- [31] P Kinsler, M Fernée, and PD Drummond. Limits to squeezing and phase information in the parametric amplifier. *Physical Review A*, 48(4):3310, 1993.
- [32] Zeev Ditzian. Relating smoothness to expressions involving fourier coefficients or to a fourier transform. *Journal of Approximation Theory*, 164(10):1369–1389, 2012.
- [33] Juan José Rodríguez-Aldavero, Paula García-Molina, Luca Tagliacozzo, and Juan José García-Ripoll. Chebyshev approximation and composition of functions in matrix product states for quantum-inspired numerical analysis. *arXiv preprint arXiv:2407.09609*, 2024.
- [34] A Bandilla, G Drobný, and I Jex. Parametric down-conversion and maximal pumpdepletion. *Journal of Optics B: Quantum and Semiclassical Optics*, 2(3):265, 2000.
- [35] Michael Fleischhauer and Oliver Veits. Long-time dynamics of spontaneous parametric down-conversion and quantum limitations of conversion efficiency. *Zeitschrift für Naturforschung A*, 54(1):57–62, 1999.
- [36] Mark Hillery and M Suhail Zubairy. Path-integral approach to the quantum theory of the degenerate parametric amplifier. *Physical Review A*, 29(3):1275, 1984.
- [37] David D Crouch and Samuel L Braunstein. Limitations to squeezing in a parametric amplifier due to pump quantum fluctuations. *Physical Review A*, 38(9):4696, 1988.
- [38] Z Vernon and JE Sipe. Strongly driven nonlinear quantum optics in microring resonators. *Physical Review A*, 92(3):033840, 2015.
- [39] Dmitry V Strekalov, Christoph Marquardt, Andrey B Matsko, Harald GL Schwefel, and Gerd Leuchs. Nonlinear and quantum optics with whispering gallery resonators. *Journal of Optics*, 18(12):123002, 2016.
- [40] Arslan S Raja, Andrey S Voloshin, Hairun Guo, Sofya E Agafonova, Junqiu Liu, Alexander S Gorodnitskiy, Maxim Karpov, Nikolay G Pavlov, Erwan Lucas, Ramzil R Galiev, et al. Electrically pumped photonic integrated soliton microcomb. *Nature communications*, 10(1):680, 2019.
- [41] Tobias Herr, Klaus Hartinger, Johann Riemensberger, Christine Y Wang, Emanuel Gavartin, Ronald Holzwarth, Michael L Gorodetsky, and Tobias J Kippenberg. Universal formation dynamics and noise of kerr-frequency combs in microresonators. *Nature photonics*, 6(7):480–487, 2012.
- [42] Alexander K. Vorobyev, Nikolay A. Kapridov, Timur R. Yunusov, Danila V. Morozov, Andrei N. Danilin, Alexey D. Ivanov, Artem E. Shitikov, Valery E. Lobanov, Igor A. Bilenko, and Dmitry A. Chermoshentsev. Optimization of the dual-pumped normal-dispersion integrated parametric oscillator in the presence of thermal effects. *Physical Review Applied*, 2025.

- [43] Nadezhda S Tatarinova, Artem E Shitikov, Georgy V Grechko, Alexander K Vorobyev, Anatoly V Masalov, Igor A Bilenko, Dmitry A Chermoshentsev, and Valery E Lobanov. Optimization of the threshold for degenerate optical parametric oscillations in a bichromatically pumped microresonator. *Physical Review Applied*, 24(2):024010, 2025.
- [44] Jutho Haegeman, J Ignacio Cirac, Tobias J Osborne, Iztok Pizorn, Henri Verschelde, and Frank Verstraete. Time-dependent variational principle for quantum lattices. *Physical review letters*, 107(7):070601, 2011.
- [45] Christian Lubich, Ivan V Oseledets, and Bart Vandereycken. Time integration of tensor trains. *SIAM Journal on Numerical Analysis*, 53(2):917–941, 2015.
- [46] Jutho Haegeman, Christian Lubich, Ivan Oseledets, Bart Vandereycken, and Frank Verstraete. Unifying time evolution and optimization with matrix product states. *Physical Review B*, 94(16):165116, 2016.
- [47] Lieven De Lathauwer, Bart De Moor, and Joos Vandewalle. A multilinear singular value decomposition. *SIAM journal on Matrix Analysis and Applications*, 21(4):1253–1278, 2000.
- [48] Ledyard R Tucker. Some mathematical notes on three-mode factor analysis. *Psychometrika*, 31(3):279–311, 1966.
- [49] Y-Y Shi, L-M Duan, and Guifre Vidal. Classical simulation of quantum many-body systems with a tree tensor network. *Physical Review A—Atomic, Molecular, and Optical Physics*, 74(2):022320, 2006.

V. APPENDIX

A. MPO for \hat{a} and \hat{a}^\dagger operators

In the continuous representation, creation and annihilation operators are written as

$$\begin{cases} \hat{a}^\dagger = \frac{\hat{X} - d/dX}{\sqrt{2}}, \\ \hat{a} = \frac{\hat{X} + d/dX}{\sqrt{2}}. \end{cases} \quad (9)$$

The position operator \hat{X} for the interval $[x_a, x_b]$ is discretized with a step size $\Delta x = (x_b - x_a)/(2^n - 1)$, has the following matrix representation

$$X = \begin{pmatrix} x_1 & 0 & \cdots & 0 \\ 0 & x_2 & \cdots & 0 \\ \vdots & \vdots & \ddots & \vdots \\ 0 & 0 & \cdots & x_N \end{pmatrix}, \quad (10)$$

where $x_k = x_a + (k-1)\Delta x$ for $k = 1, 2, \dots, N = 2^n$. It can be shown that this matrix can be represented as an MPO:

$$X = A_1 A_2 \cdots A_{n-1} A_n \quad (11)$$

where

$$A_1 = \begin{pmatrix} (1 & 0) & (0 & 0) \\ (0 & 1) & (0 & 1) \end{pmatrix}, \quad (12)$$

$$A_2, \dots, A_{n-1} = \begin{pmatrix} \begin{pmatrix} (1 & 0) & (0 & 0) \\ (0 & 1) & (0 & 1) \\ (0 & 0) & (2 & 0) \\ (0 & 0) & (0 & 2) \end{pmatrix} \end{pmatrix}, \quad (13)$$

$$A_n = \begin{pmatrix} \begin{pmatrix} x_a & 0 \\ 0 & x_a + \Delta x \\ 2\Delta x & 0 \\ 0 & 2\Delta x \end{pmatrix} \end{pmatrix}. \quad (14)$$

The inner matrices of the size 2x2 correspond to physical dimension. The outer matrix which contains smaller ones as its elements correspond to bond dimension.

Similarly, the matrix representation of the first derivative is approximated by the second-order central difference:

$$D^{(1)} = \frac{1}{2\Delta x} \begin{pmatrix} 0 & 1 & 0 & \cdots & 0 \\ -1 & 0 & 1 & \cdots & 0 \\ 0 & -1 & 0 & \cdots & 0 \\ \vdots & \vdots & \vdots & \ddots & \vdots \\ 0 & 0 & \cdots & -1 & 0 \end{pmatrix}, \quad (15)$$

$$D^{(1)} = A_1 A_2 \cdots A_{n-1} A_n, \quad (16)$$

where

$$A_1 = \frac{1}{2\Delta x}, \begin{pmatrix} (1 & 0) & (0 & 1) & (0 & 0) \\ (0 & 1) & (0 & 0) & (-1 & 0) \end{pmatrix}, \quad (17)$$

$$A_2, \dots, A_{n-1} = \begin{pmatrix} \begin{pmatrix} (1 & 0) & (0 & 1) & (0 & 0) \\ (0 & 1) & (0 & 0) & (-1 & 0) \\ (0 & 0) & (0 & 0) & (0 & 0) \\ (0 & 0) & (1 & 0) & (0 & 0) \\ (0 & 0) & (0 & 0) & (0 & 1) \\ (0 & 0) & (0 & 0) & (0 & 0) \end{pmatrix} \end{pmatrix}. \quad (18)$$

$$A_n = \begin{pmatrix} \begin{pmatrix} (0 & 1) \\ (-1 & 0) \\ (0 & 0) \\ (1 & 0) \\ (0 & 1) \\ (0 & 0) \end{pmatrix} \end{pmatrix} \quad (19)$$

B. Solving systems of linear equations within MPS representation

The variational method provides an efficient approach for solving systems of linear equations directly in the MPS format. For this purpose, we construct a functional (20) (Fig. 4(b)) whose global minimum corresponds to the solution of a system of linear equations (3) (Fig. 4(a)).

$$J = \frac{1}{2} \psi_{t+1}^* U \psi_{t+1} - \psi_{t+1}^* \psi_t, \quad (20)$$

To minimize this functional, the tensors of ψ_{t+1} MPS are initialized in some initial state and then iteratively optimized. By sequentially updating local tensor pairs, the problem reduces to solving small linear systems (in Fig. 4(c, d) the update of second and third tensors in MPS is illustrated), significantly lowering computational complexity and memory consumption. The update of a tensor pair is performed by solving a reduced system of equations (21) (Fig. 4(d)).

$$U'x - b = 0 \quad (21)$$

where x is a vector determined by the tensor pair we seek.

Once x is obtained, it is decomposed into two separate tensors. This operation is done by reshaping x into a matrix of the appropriate form and applying singular value decomposition (SVD) (Fig. 4(e)). Importantly, if all tensors to the left of a given pair are left-normalized and all tensors to the right are

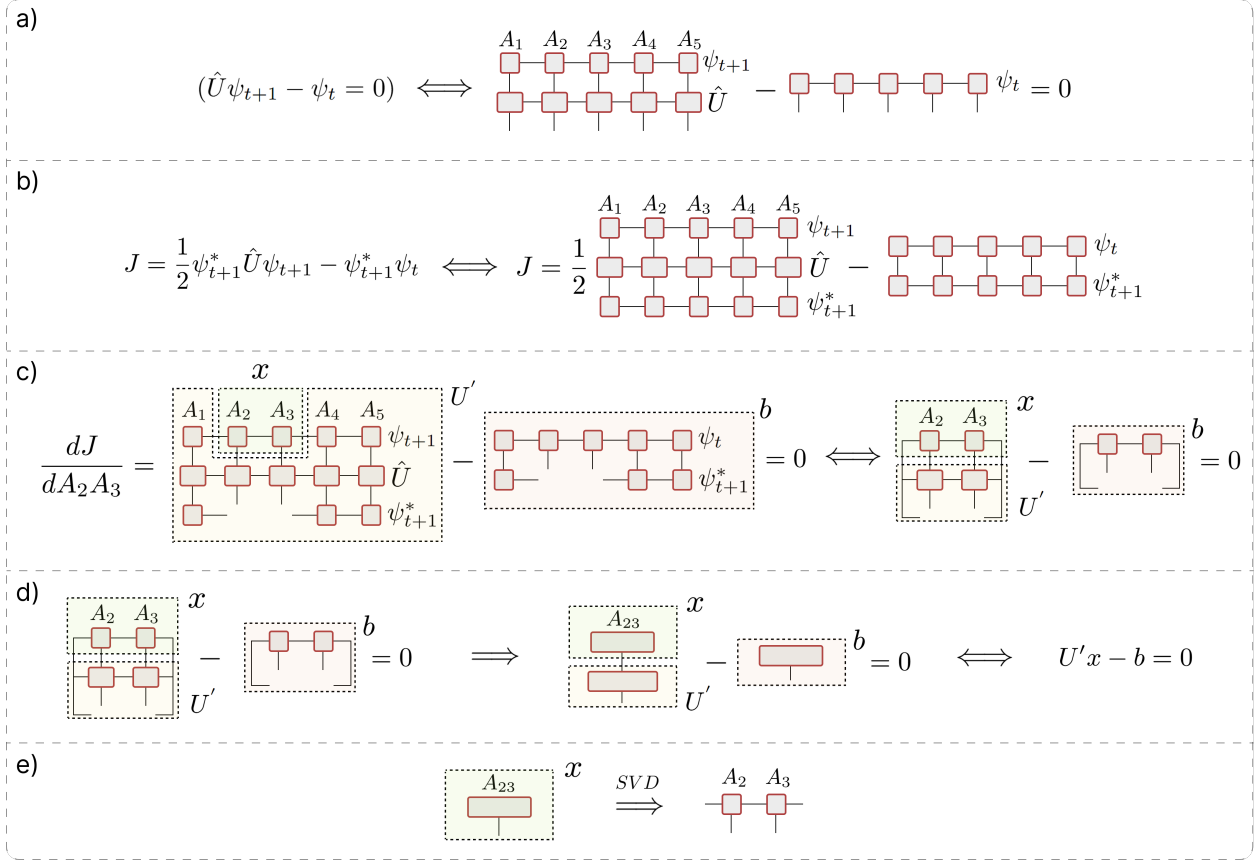


FIG. 4. Diagrammatic illustration of DMRG style algorithm for solving linear systems in the MPS format. (a) System of linear equations in the MPS form; (b) Functional which global minimum corresponds to the solution of a linear system of equations. (c) Variation of the functional with respect to a pair of MPS tensors. (d) Local linear system for the corresponding pair of tensors.

right-normalized, then the SVD provides a Schmidt decomposition of the MPS. This allows us to properly truncate the smallest singular values while ensuring that the resulting error remains small.

After computing a new pair of tensors, one of them is fixed while the second and a subsequent tensor are varied. In this manner, all tensors in the tensor network are sequentially updated. The process of updating all tensors in the network from one edge to another is called sweep. To achieve convergence of the algorithm, multiple sweeps are required. When updating a pair of tensors in this way, the bond dimension is adjusted automatically.

Fig. 3(b) demonstrates the amount of information needed to store MPS states in memory compared to the mesh size.